Taylor & Francis
Taylor & Francis Group

RESEARCH PAPER

BIRC5/Survivin is a novel ATG12–ATG5 conjugate interactor and an autophagy-induced DNA damage suppressor in human cancer and mouse embryonic fibroblast cells

Tzu-Yu Lin [a], Hsiu-Han Chan [b], Shang-Hung Chen [c,d*], Sailu Sarvagalla [e*], Pai-Sheng Chen [a,f], Mohane Selvaraj Coumar [e], Siao Muk Cheng [a], Yung-Chieh Chang [a], Chun-Hui Lin [b], Euphemia Leung [g], and Chun Hei Antonio Cheung [a,b]

aInstitute of Basic Medical Sciences, College of Medicine, National Cheng Kung University, Tainan, Taiwan; bDepartment of Pharmacology, College of Medicine, National Cheng Kung University, Tainan, Taiwan; cNational Institute of Cancer Research, National Health Research Institutes, Tainan, Taiwan; dDivision of Hematology and Oncology, Department of Internal Medicine, National Cheng Kung University Hospital, College of Medicine, National Cheng Kung University, Tainan, Taiwan; eCentre for Bioinformatics, School of Life Sciences, Pondicherry University, Puducherry, India; fDepartment of Medical Laboratory Science and Biotechnology, College of Medicine, National Cheng Kung University, Tainan, Taiwan; gAuckland Cancer Society Research Centre and Department of Molecular Medicine and Pathology, University of Auckland, Auckland, New Zealand

ABSTRACT

BIRC5/Survivin is known as a dual cellular functions protein that directly regulates both apoptosis and mitosis in embryonic cells during embryogenesis and in cancer cells during tumorigenesis and tumor metastasis. However, BIRC5 has seldom been demonstrated as a direct macroautophagy/autophagy regulator in cells. ATG7 expression and ATG12–ATG5-ATG16L1 complex formation are crucial for the phagophore elongation during autophagy in mammalian cells. In this study, we observed that the protein expression levels of BIRC5 and ATG7 were inversely correlated, whereas the expression levels of BIRC5 and SQSTM1/p62 were positively correlated in normal breast tissues and tumor tissues. Mechanistically, we found that BIRC5 negatively modulates the protein stability of ATG7 and physically binds to the ATG12–ATG5 conjugate, preventing the formation of the ATG12–ATG5-ATG16L1 protein complex in human cancer (MDA-MB-231, MCF7, and A549) and mouse embryonic fibroblast (MEF) cells. We also observed a concurrent physical dissociation between BIRC5 and ATG12–ATG5 (but not CASP3/caspase-3) and upregulation of autophagy in MDA-MB-231 and A549 cells under serum-deprived conditions. Importantly, despite the fact that upregulation of autophagy is widely thought to promote DNA repair in cells under genotoxic stress, we found that BIRC5 maintains DNA integrity through autophagy negative-modulations in both human cancer and MEF cells under non-stressed conditions. In conclusion, our study reveals a novel role of BIRC5 in cancer cells as a direct regulator of autophagy. BIRC5 may act as a "bridging molecule", which regulates the interplay between mitosis, apoptosis, and autophagy in embryonic and cancer cells.

Abbreviations: ACTA1: actin; ATG: autophagy related; BIRC: baculoviral inhibitor of apoptosis repeat-containing; BAF: bafilomycin A_1; CQ: chloroquine; CASP3: caspase 3; HSPB1/Hsp27: heat shock protein family B (small) member 1/heat shock protein 27; IAPs: inhibitors of apoptosis proteins; IP: immunoprecipitation; MAP1LC3/LC3: microtubule associated protein 1 light chain 3; PLA: proximity ligation assay; SQSTM1/p62: sequestosome 1; siRNA: small interfering RNA

Introduction

Macroautophagy (hereafter referred to as autophagy) is a lysosomal degradation pathway for the breakdown of intracellular proteins and organelles [1]. Despite various efforts have been made in the past ten years in dissecting the differential functions and the related underlying regulations of autophagy in different cellular conditions; our understanding on the molecular regulatory mechanisms of autophagy is still far from complete.

BIRC5 is a member of the inhibitor-of-apoptosis proteins (IAPs) family discovered in 1997 [2]. It is highly expressed in embryonic tissues (*e.g.* neuronal precursor cells and embryonic fibroblasts) and tumors (including both cancer cells and cancer stem cells), and its expression is associated with tumor cell differentiation, proliferation, invasion, and metastasis [3–11]. Interestingly, a few studies revealed that BIRC5 also plays an important role in neural cell proliferation after traumatic brain injury and in cardiomyocytes survival maintenance after cardiac injury [12–15]. At the molecular level, like other baculovirus IAP repeat (BIR) domain containing IAPs family members, BIRC5 binds to caspases and inhibits their activities in cells [16,17]. On the other hand, BIRC5 promotes mitosis through formation of the chromosomal passenger complex (CPC) with CDCA8/Borealin, AURKB (aurora B kinase) and INCENP (inner centromere protein), and regulation of the microtubule dynamics during G_2/M phase in proliferating cells [18,19]. Accordingly, BIRC5 also interacts with AURKC (aurora C kinase) to promote mitosis [20].

Given the roles of BIRC5 in apoptosis and mitosis regulation, targeting BIRC5 shall induce cell cycle arrest, caspases activation, and apoptosis in cancer cells [21]. Surprisingly, a few research groups including us found that YM155 (sepantronium bromide), which is a first-in-class BIRC5 small molecule suppressant [22,23], induced autophagy-dependent DNA damage and autophagic cell death in cancer cells regardless of the status/expression of TP53/p53 and CASP3 [24–26]. Our research group also found in a previous study that SAHA (vorinostat, a pan-HDAC inhibitor) induced autophagy in part through BIRC5 downregulation in breast cancer cells [27]. These phenomena are indeed interesting and suggest that BIRC5 may exhibit an autophagy regulatory function, which has yet to be discovered. In this study, we discovered that BIRC5 is a novel ATG12–ATG5 conjugate interactor that negatively regulates autophagy and suppresses autophagy-induced DNA damage in human cancer cells.

Results

### BIRC5 negatively modulates autophagy in human cancer and mouse embryonic fibroblast cells

We previously demonstrated that liposomal delivery of an antisense BIRC5-expressing plasmid DNA increased LC3B-II conversion and LC3 puncta formation (markers for autophagosomes/autolysosomes) in human cancer cells [28]. Here, we sought to first confirm the effects of BIRC5 expression alteration on autophagy in cells with different tissue origins and CASP3 expression status. Results of the western blot analysis showed that BIRC5 downregulation by siRNA promoted LC3B-II conversion and decreased SQSTM1 expression (an autophagic substrate) in MDA-MB-231 (CASP3-expressing breast cancer cell line), MCF7 (CASP3-deficient breast cancer cell line), A549 (CASP3-expressing lung cancer cell line), and mouse embryonic fibroblast (MEF) cells (Figure 1A and S1A). BIRC5 downregulation also decreased the protein stability of SQSTM1 (dynamic marker for autophagic flux induction) and increased the number of LC3 puncta and acidic vesicular organelles (AVOs; i.e. autolysosome and/or lysosome) present in MDA-MB-231 cells (Figure S1B and S1C, Figure 1B) [29]. Moreover, results of the fluorescence microscopy and western blot analysis showed that the number of the yellow (i.e. autophagosome) and red fluorescent (i.e. autolysosome) LC3 puncta was increased in the mRFP-EGFP-LC3 expressing MDA-MB-231 cells treated with BIRC5 siRNA (Figure 1C) and the conversion of LC3B-II was further increased in cells co-treated with BIRC5 siRNA and CQ (Figure S1D), respectively, supporting that BIRC5 downregulation increases autophagic flux in cells. In contrast, ectopic overexpression of BIRC5 decreased LC3B-II conversion, and increased the transcription-independent SQSTM1 expression in the treated cells (Figure 1D,E). Resveratrol is an autophagy inducer and ATG7 is a molecule known to play an important role in autophagosome formation during canonical autophagy [30,31]. Results of the western blot analysis and fluorescence microscopy showed that ectopic overexpression of BIRC5 attenuated the effects of resveratrol on LC3B-II conversion, SQSTM1 and ATG7 expression, LC3 puncta and AVOs formation in MDA-MB-231 cells (Figure 1F-H). Overexpression

of BIRC5 also attenuated the effect of resveratrol on the formation of the yellow (greenish-yellow) and red fluorescent LC3 puncta in the mRFP-EGFP-LC3-expressing MDA-MB-231 cells, confirming that BIRC5 overexpression inhibits autophagic flux in cells (Figure 1I).

The relationship between BIRC5 expression and the baseline autophagy levels was subsequently examined in clinical samples by analyzing the expression of BIRC5, ATG7, and SQSTM1 on sections (tissue array; SUPER BIO CHIPS – CBB3) of breast cancer tissue (n = 30) and the respective normal breast tissue (n = 30) using immunohistochemical analysis. In mammalian cells, ATG7 is an E1-like enzyme that facilitates the conjugation between ATG12 and ATG5 (Figure 2A), which is a prerequisite event for the formation of ATG12–ATG5-ATG16L complex and the lipidation of LC3 (i.e. LC3B-II conversion) [32–34]. Consistent with our hypothesized negative-modulatory role of BIRC5 on autophagy, the immunoreactive expression levels of BIRC5 and ATG7 were inversely correlated, whereas the expression levels of BIRC5 and SQSTM1 were positively correlated between normal breast tissues and tumor tissues (Figure 2B-D). Collectively, these results support that BIRC5 is a negative-modulator of autophagy.

BIRC5 negatively modulates ATG7 expression and ATG12–ATG5 conjugation in human cancer and mouse embryonic fibroblast cells

The molecular chaperone, HSPB1/Hsp27, has been found as a positive-regulator of the amount of ATG7 protein present in Drosophila cells and human glioblastoma cells [35,36]. Intriguingly, ectopic overexpression of BIRC5 decreased the expression of HSPB1 and increased the amount of the ubiquitinated-ATG7 present in the examined cells (i.e. MDA-MB-231 and A549) (Figure S2A and S2B). Furthermore, immunoprecipitation of the endogenous ATG7 revealed that ATG7 interacts with HSPB1 in MDA-MB-231 cells (Figure S2C). Together with the results of our pilot study showing that Birc5 downregulation increased Atg7 expression in MEF cells (Figure S2D), we hypothesized that BIRC5 might directly regulate autophagy through ATG7 modulation. Results of the western blot analysis showed that BIRC5 downregulation by siRNA increased ATG7 expression and ATG12–ATG5 conjugation in MDA-MB-231, MCF7, and A549 cells (Figure 3A, left and middle panels). BIRC5 downregulation by the known BIRC5 expression suppressant, YM155, also increased ATG7 expression and ATG12–ATG5 conjugation in the treated human cancer cells (Figure S3A). Conversely, ectopic BIRC5 overexpression decreased ATG7 expression and ATG12–ATG5 conjugation in MDA-MB-231, MCF7, and A549 cells (Figure 3A, right panels). To determine whether the BIRC5 siRNA (or YM155)-induced ATG7 overexpression was indirectly caused by a positive feedback signaling during autophagy activation, we examined the effects of Birc5 downregulation on Atg7 expression in the autophagy-deficient, $atg5^{-/-}$ MEF cells. As shown in Figure S3B, $atg5^{-/-}$ MEF cells did not express Atg12–Atg5 conjugate and LC3B-II as expected. Downregulation of mouse Birc5 by siRNA increased the expression of ATG7 independent of ATG5 and ATG12–ATG5 conjugate as shown in $atg5^{-/-}$ MEF cells.
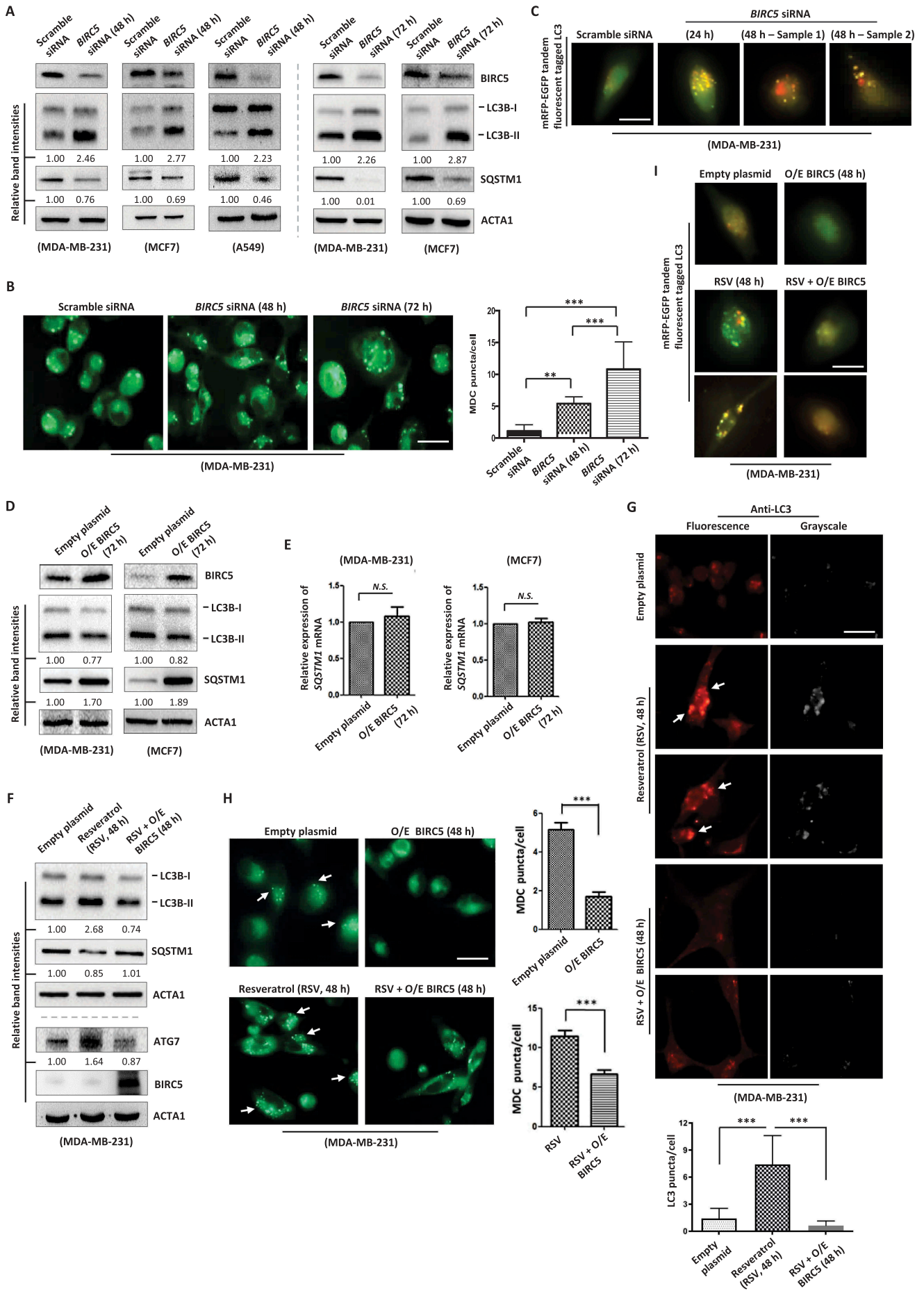
MTOR (mechanistic target of rapamycin kinase) is a well-known autophagy initiation negative-regulator and RUBCN (rubicon autophagy regulator) is an autophagosome maturation inhibitor. Here, ectopic BIRC5 overexpression did not alter the amount (*i.e.* < 10% changes) of p-MTOR and RUBCN present in MDA-MB-231 and MCF7 cells (**Figure S3C**), indicating that BIRC5 modulates autophagy mostly through an MTOR/RUBCN-independent mechanism. BIRC5 binds to AURKB/AURKC and regulates mitosis in cancer cells [18,19]. Here, contrast to the targeting *BIRC5* by siRNA and YM155, inhibiting Aurora kinases by VX680 did not increase the amount of ATG12–ATG5 conjugate present in MDA-MB-231 cells (**Figure S3D**). Moreover, ectopic over-expression of another IAPs family protein, BIRC3/cIAP2 (baculoviral IAP repeat containing 3), did not alter the expression of ATG7 and ATG12–ATG5 conjugate, and the conversion of LC3B-II (**Figure S3E**) to the levels as observed in MDA-MB-231 cells with ectopic overexpression of BIRC5 (Figure 3A, **right panels**). Taken together, these results indicate that the effects on ATG7 and ATG12–ATG5 conjugate expression observed in BIRC5 downregulation and the ectopic BIRC5 overexpression experiments were BIRC5-specific and independent of its roles on mitosis.

BIRC5 modulates ATG7 expression at the post-translational level

We further investigated the ATG7 expression modulatory mechanism of BIRC5 in MDA-MB-231, MCF7, and A549 cells. ATG7 is a long-lived (half-life > 96 h) protein in cells. Results of the qPCR analysis showed that overexpression (and downregulation) of BIRC5 did not alter the amount of *ATG7* mRNA transcripts present in all cell lines tested (Figure 3B). In contrast to the results of the qPCR analysis and in align with the results of the ATG7 ubiquitination analysis (**Figure S2B**), ectopic overexpression of BIRC5 promoted the degradation of ATG7 protein in MDA-MB-231 (*i.e.* 24 and 36 h post cycloheximide [CHX] incubation) and A549 (*i.e.* 36 h post CHX incubation) cells (Figure 3C). Inhibition of the proteasomal protein degradation pathway by MG132 restored (largely enhanced) ATG7 expression in BIRC5-overexpressed MDA-MB-231 and A549 cells (**Figure S3F**), confirming that BIRC5 regulates ATG7 expression through proteasome-related protein stability modulation.

BIRC5 interacts with ATG12–ATG5 conjugate

Hypothetically, any protein that binds to either ATG12 or ATG5 monomer can potentially affect the conjugation between ATG12 and ATG5. Surprisingly, even though the expression of ATG12–ATG5 conjugate began to increase at 12 h post-YM155 treatment, the expression of ATG7 remains unchanged at the same time-point in A549 cells, suggesting that BIRC5 might also regulate ATG12–ATG5 conjugation through an ATG7-independent mechanism (**Figure S3A**). Therefore, we examined the possibility on protein complexation between BIRC5, ATG12, and ATG5 using computational analysis (protein-protein docking followed by molecular dynamics simulation) (Figure 4A). Intriguingly, results of the computational analysis suggested that BIRC5 could form protein complex with the unconjugated ATG12 (*i.e.* ATG12-BIRC5 protein complex) and ATG5 monomer (*i.e.* ATG5-BIRC5 protein complex) and competitively interfere with the formation of ATG12–ATG5 conjugate (Figure 4B). Our computational models also suggested that BIRC5 could form complex with ATG12–ATG5 conjugate (*i.e.* ATG12–ATG5-BIRC5 protein complex) and competitively interfere with the formation of ATG12–ATG5-ATG16L1 protein complex (Figure 4B). Complete descriptions of the computational modeling results are listed in **supplementary information (SI) – S2.1, Figure S4-S7, and Table S1-S3**.

To validate the existence of the ATG12-BIRC5, ATG5-BIRC5, and ATG12–ATG5-BIRC5 protein complexes, proteins were extracted from MDA-MB-231, A549, and MCF7 cells and subjected to immunoprecipitation with anti-BIRC5, anti-ATG12, and anti-ATG5 antibodies. Immunoprecipitation of the endogenous BIRC5 revealed that BIRC5 interacts with ATG12–ATG5 conjugate (Figure 5A, **left panel, and S8A, left panel**). Unfortunately, only ATG12–ATG5 conjugate, but not the unconjugated-ATG5 monomer containing immune-complexes, was successfully extracted using immunoprecipitation with anti-ATG5 antibody (Figure 5A, **middle panel**). Results of the reciprocal immunoprecipitation analysis again showed that BIRC5 interacts with ATG12–ATG5 conjugate/unconjugated ATG12 in MDA-MB-231 and MCF7 cells (Figure 5A, **middle and right panels, and Figure S8A, right panel**).

We suspected that the failure of using immunoprecipitation to extract the unconjugated-ATG5-containing protein complex (Figure 5A, **middle panel**) and the absent of the unconjugated-ATG12 monomer band on blots (**Figure S8A**) were due to the low expression level of the unconjugated-ATG5 and -ATG12

Figure 1. BIRC5 modulates autophagy in cancer cells. (A) Cancer cells were transfected with either scramble siRNA or *BIRC5* siRNA for 48–72 h. Expression of different proteins was determined by western blotting. ACTA1/actin was used as an internal control. (B) MDA-MB-231 cells were transfected with either scramble siRNA or *BIRC5* siRNA for indicated durations. Cells were stained with MDC and formation of AVOs was determined using fluorescence microscopy. A statistically significant difference in the amount of AVOs present in cells between the testing groups is denoted by "**" ($p < 0.01$) and "***" ($p < 0.001$). (C) The mRFP-EGFP-LC3 expressing (from the plasmid DNA – ptfLLC3) MDA-MB-231 cells were transfected with either scramble siRNA or *BIRC5* siRNA for the indicated durations. Formation of green and red fluorescent LC3 puncta was determined using fluorescence microscopy. Images shown in this panel were the "merged-images" of the green and red fluorescence images. (D) MDA-MB-231 and MCF7 cells were transfected with either the pCMV6-XL4 plasmid DNA (Empty plasmid) or the pCMV6-XL4-*BIRC5* plasmid DNA (O/E BIRC5; O/E – ectopic expressing) for 72 h. Expression of different proteins was determined by western blotting. ACTA1 was used as an internal control. (E) Cells were transfected with either the empty plasmid DNA or the BIRC5 expressing pCMV6-XL4-*BIRC5* plasmid DNA for 72 h. The relative amount of *SQSTM1* mRNA transcripts present in cells was determined by qPCR. A "*N.S.*" denotes no statistical significance difference between the testing groups. (F and G) MDA-MB-231 cells were transfected with either the empty plasmid DNA or the BIRC5-expressing pCMV6-XL4-*BIRC5* plasmid DNA with or without resveratrol co-treatment for 48 h. Expression of different proteins and the formation of LC3 puncta was determined by western blotting and fluorescence microscopy, respectively. (H) Cells were stained with MDC and formation of AVOs was determined using fluorescence microscopy. A statistically significant difference in the amount of AVOs present in cells between the testing groups is denoted by "***" ($p < 0.001$). (I) The mRFP-EGFP-LC3 expressing MDA-MB-231 cells were treated with or without resveratrol for 48 h. Formation of green and red fluorescent LC3 puncta was determined using fluorescence microscopy. Images shown in this panel were the "merged-images" of the green and red fluorescence images. Scale bars: 30 μm (B, G, and H), 25 μm (C and I).
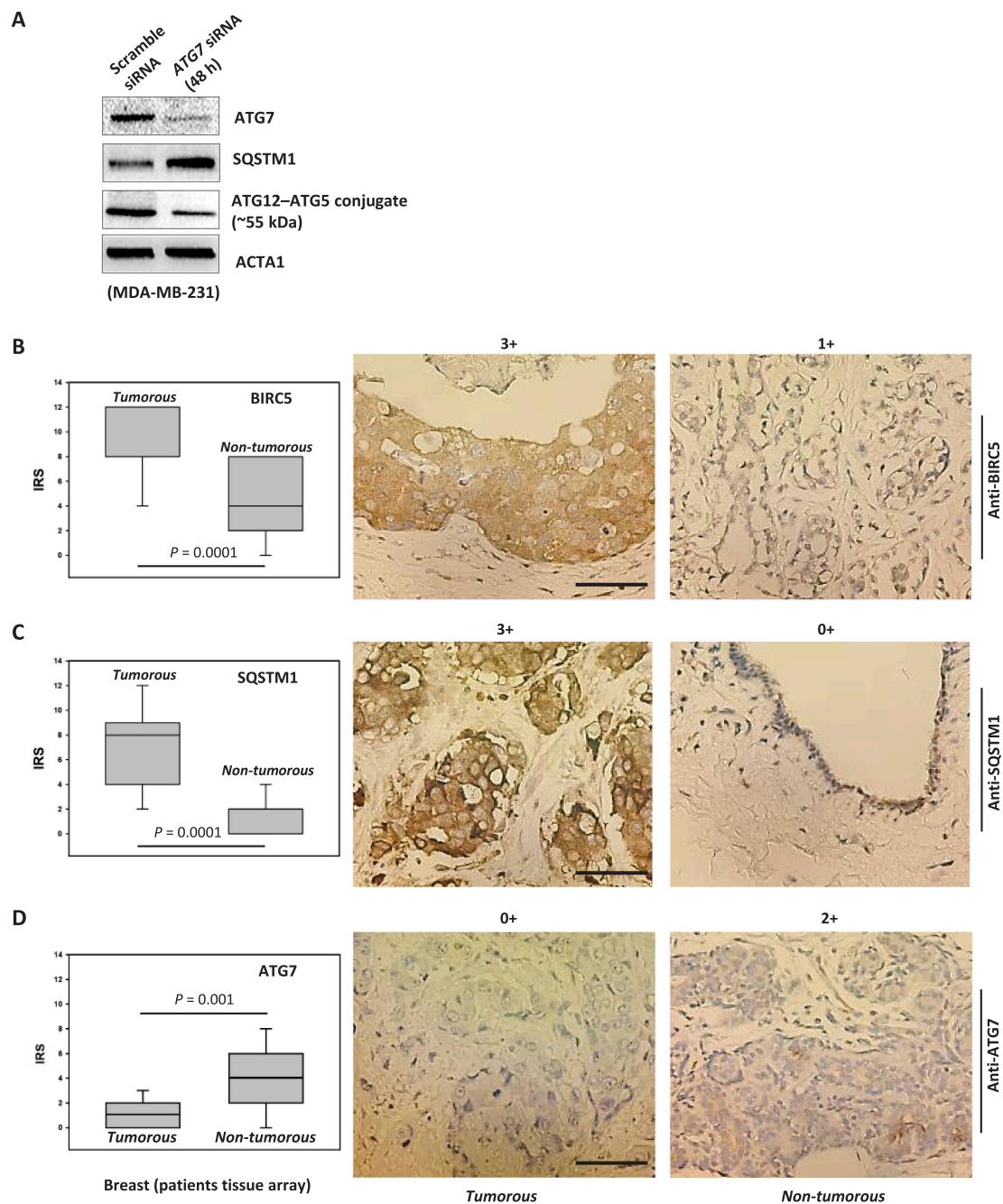
Figure 2. BIRC5 expression and the baseline autophagy levels exhibit inverse correlations in clinical samples. (A) MDA-MB-231 cells were transfected with either the scramble siRNA or *ATG7* siRNA for 48 h. Expression of different proteins was determined by western blotting. (B, C, and D) The expression levels of BIRC5, SQSTM1 and ATG7 were immunohistochemically accessed based on staining density and intensity using the immunoreactive score (IRS) system. Shown are IRS comparisons (left panel) and representative immunohistochemical staining (right panel) reflecting expression levels of these three proteins in tumorous and non-tumorous tissues. The comparisons between protein expression levels were performed using one-way ANOVA. Scale bar: 60 μm (B, C, and D).

monomer in MDA-MB-231 and A549 cells, respectively (**Figure S8B**). As the detection sensitivity for protein-protein interactions of the endogenous co-immunoprecipitation assay is limited, the highly sensitive *in situ* proximity ligation assay (PLA) was used. First, we determined the subcellular localization of ATG12–ATG5 conjugate, ATG12, and ATG5 monomer in cells. Despite results of the immunofluorescence microscopy showed that ATG5- and ATG12-related green fluorescent signals (*i.e.* representing ATG5/ATG5-containing complexes and ATG12/ATG12-containing complexes, respectively) were present in

both the cytoplasm and nucleus of MDA-MB-231 and A549 cells (Figure 5B and S8C), the red fluorescent PLA puncta representing direct protein-protein interactions between ATG12, ATG5, and ATG16L1 were located only in the cytoplasm of the cells (Figure 5C and S8D), indicating that ATG12–ATG5 conjugate (and any ATG12/ATG5 containing complexes like ATG12–ATG5-ATG16L1) is located in the cytoplasm, but not in the nucleus. Noticeably, the red fluorescent ATG12–ATG5 and ATG12-ATG16L1 PLA puncta were also observed in MEF cells but not in the *atg5*$^{-/-}$ MEF (also ATG12–ATG5 conjugate-
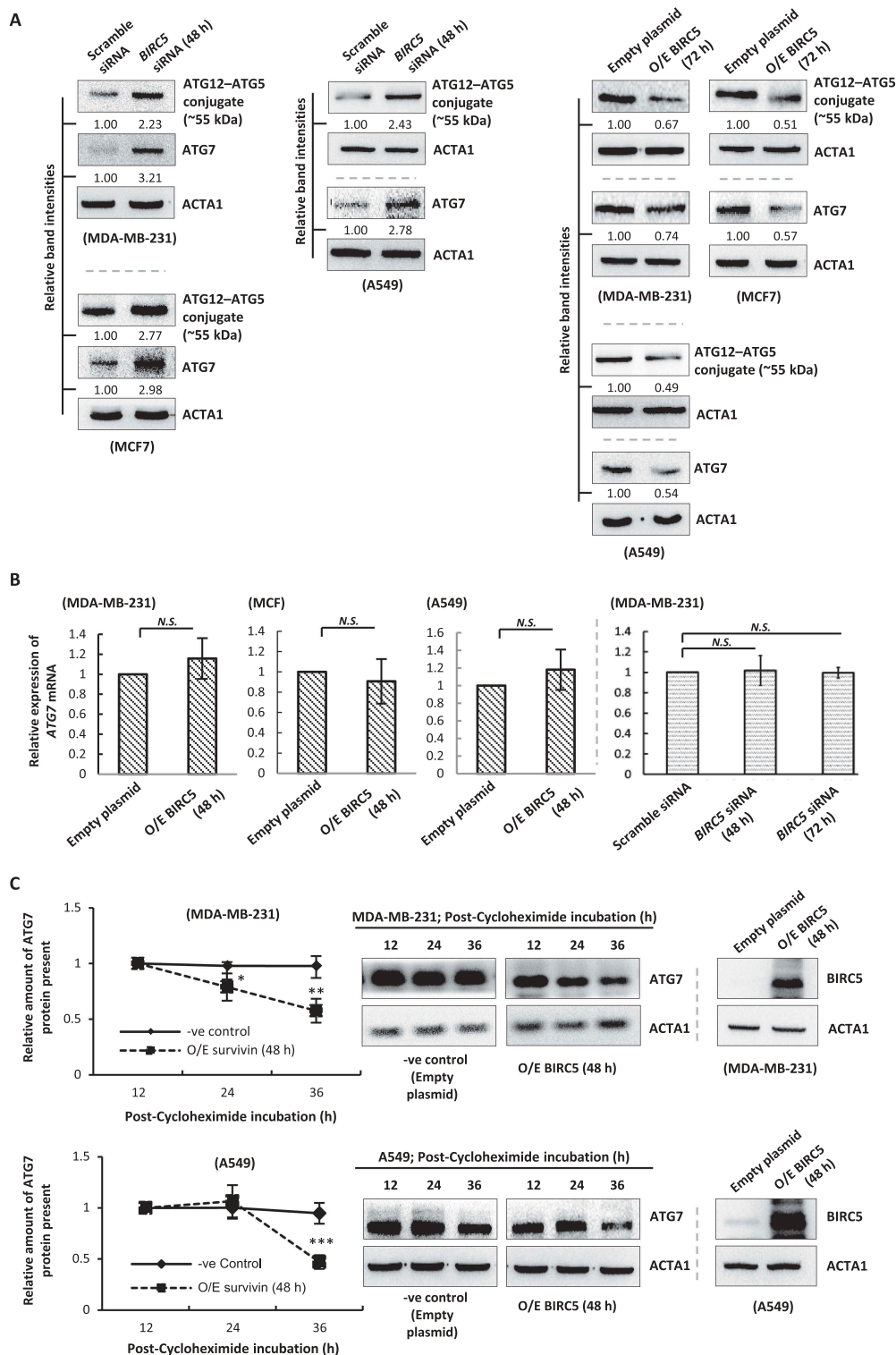
Figure 3. BIRC5 modulates the protein stability of ATG7 and the expression of ATG12–ATG5 conjugate in cancer cells. (A) Cells were transfected with the scramble siRNA, *BIRC5* siRNA, empty plasmid DNA, or the BIRC5 expressing pCMV6-XL4-*BIRC5* for the indicated durations. Expression of different proteins was determined by the western blot analysis. ACTA1 was used as an internal control. (B) Cells were transfected with the empty plasmid DNA, the BIRC5 expressing pCMV6-XL4-*BIRC5*, scramble siRNA, or *BIRC5* siRNA for 48–72 h. The relative amount of *ATG7* mRNA transcripts present in cells was analyzed by qPCR. A "*N.S.*" denotes no statistical significance difference between the testing groups. (C) MDA-MB-231 and A549 cells were transfected with either the empty plasmid DNA (-ve control) or BIRC5 expressing pCMV6-XL4-*BIRC5* (O/E BIRC5) for 48 h. Cycloheximide was added to the cells to inhibit *de novo* protein synthesis. Cells were then harvested at the time points indicated and expression of ATG7 was analyzed by western blotting. Experiments were repeated three times and representative blots were shown. Signals in the blots (of all repeats) were quantitated and a graph was generated to compare the degradation rates. A statistically significant difference in the mean of the relative band intensity (of all repeats) of ATG7 in cells transfected with the empty plasmid DNA *vs.* the BIRC5-expressing plasmid DNA at the same time point is denoted by "*" ($p < 0.05$), "**" ($p < 0.01$), or "***" ($p < 0.001$).

A

B
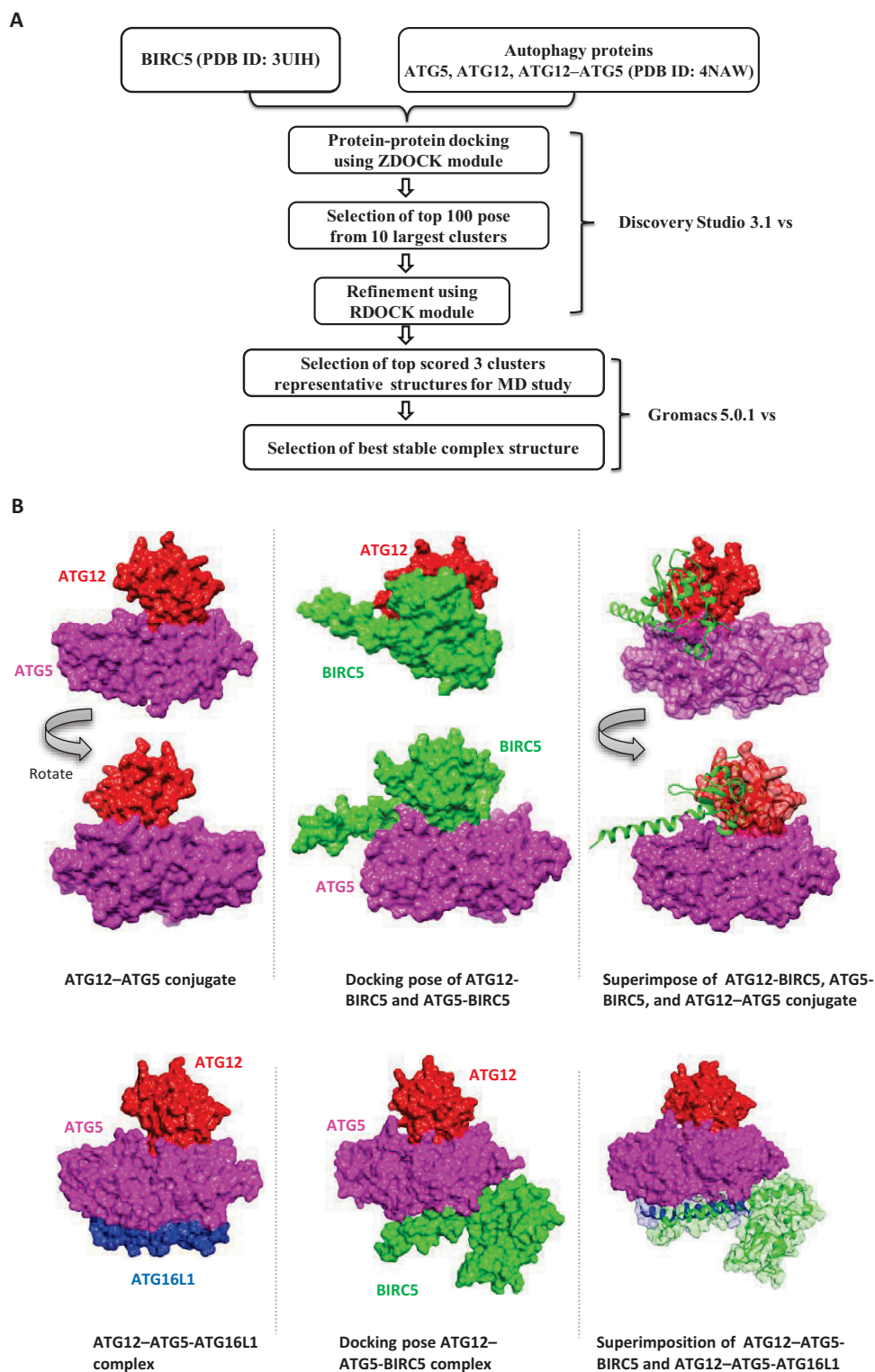
Figure 4. Computational modeling of the ATG12-BIRC5, ATG5-BIRC5, and ATG12–ATG5-BIRC5 protein complex. (A) Schematic representation of work plan to model BIRC5 interaction with ATG proteins. Please refer to the supplementary information, S1.1–1.3, for details. (B) Schematic representation of BIRC5-ATG proteins binding mode.

deficient) cells, confirming both the target-specificity of the antibodies used in this assay and the cytoplasmic localization of ATG12–ATG5 conjugate and ATG12–ATG5-ATG16L1 complex in MEF cells (Figure 5C). These findings were further confirmed by the western blot analysis showing that ATG12–ATG5 conjugate was mainly present in the cytoplasmic extract, whereas, the unconjugated-ATG12 and ATG5 were present in the nuclear extract of MDA-MB-231, A549, and MCF7 cells (Figure 5D **and S8E**). Surprisingly, the red fluorescent ATG5-BIRC5 and ATG12-BIRC5 PLA puncta were located in both the
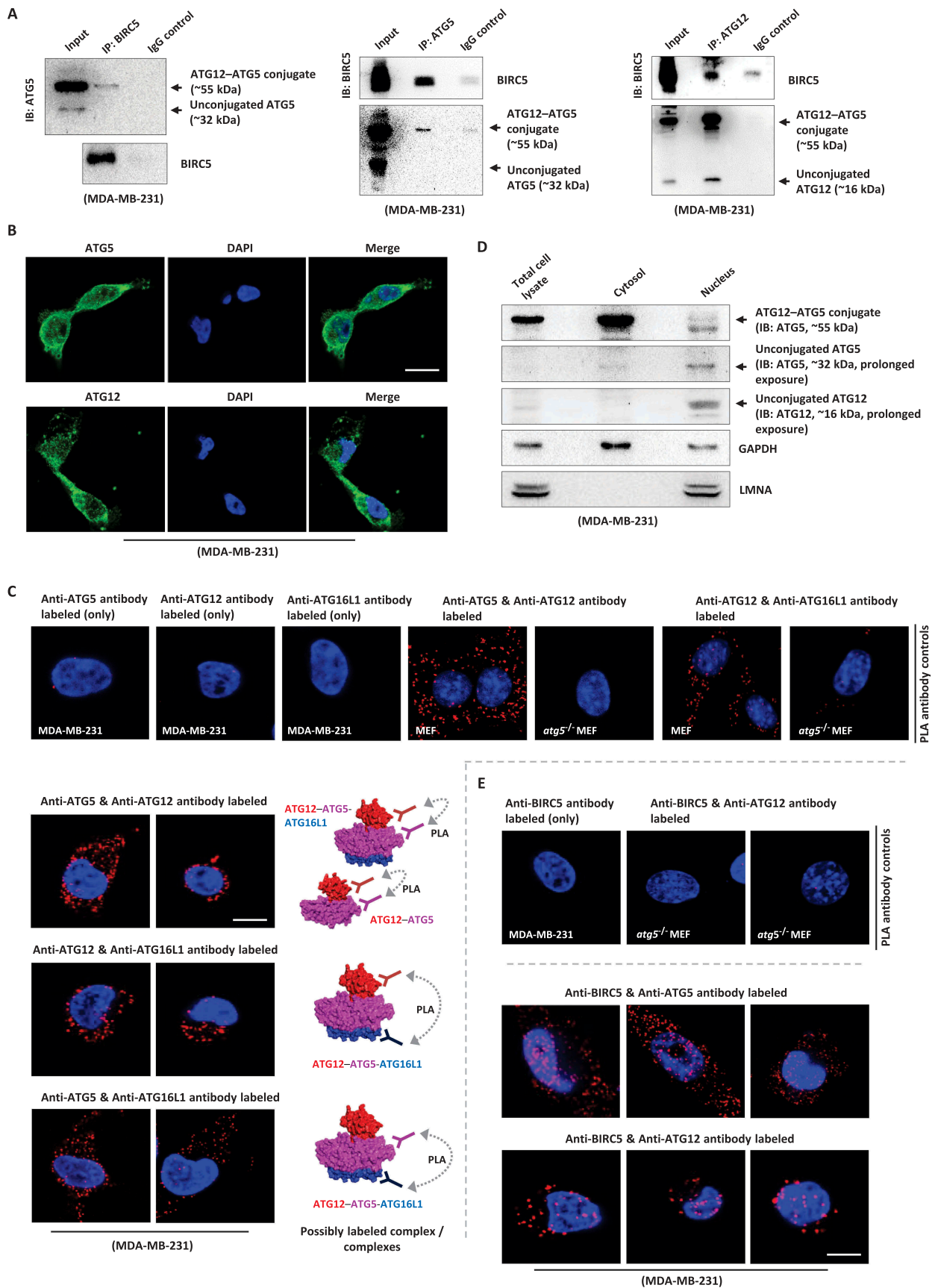
(MDA-MB-231)

cytoplasm and nucleus of MDA-MB-231, A549, and MEF cells (Figure 5E, Figure S8D and S8F). These results suggest that BIRC5 binds to ATG12–ATG5 conjugate in the cytoplasm and to the unconjugated ATG12 and ATG5 in the nucleus.

BIRC5 modulates ATG12–ATG5-ATG16L complexation in human cancer cells

Because ATG12–ATG5 conjugate, but not the unconjugated-ATG12 and ATG5 monomers, represents the major form of ATG12 and ATG5 that existed in human MDA-MB-231, MCF7, and A549 cells (Figure S8B), we decided to focus on delineating the effect of BIRC5 on the complexation between ATG12–ATG5 conjugate and ATG16L1.

According to the computational predictions, binding of BIRC5 onto ATG12–ATG5 conjugate could inhibit the physical interactions between ATG12–ATG5 conjugate and ATG16L1. Since BIRC5 has multiple binding partners such as AURKB and CASP3; therefore, it is important to determine whether ectopic overexpression of BIRC5 can increase the level of interaction between ATG12–ATG5 conjugate and BIRC5 before examining the effect of BIRC5 overexpression on ATG12–ATG5-ATG16L1 formation in cells. Even though ectopic overexpression of BIRC5 decreased the expression of ATG12–ATG5 conjugate as shown in Figure 3A and Figure S9, it increased the amount of the cytoplasmic ATG5-BIRC5 and ATG12-BIRC5 PLA puncta present in MDA-MB-231 cells (Figure 6A), suggesting that ectopic overexpression of BIRC5 could promote the formation of the ATG12–ATG5-BIRC5 protein complex. Theoretically, cytoplasmic ATG12–ATG5-ATG16L1 complexes can be detected by in situ PLA using anti-ATG5 and anti-ATG16L1 antibody as probes. However, co-expression of ATG5 and the N-terminal region of ATG16L1 (ATG16L-N) has been shown to be capable to form an ATG5-ATG16L-N protein complex in the absence of ATG12 [37,38]. Therefore, we performed in situ PLA using anti-ATG12 and anti-ATG16L1 antibody as probes to detect the formation of ATG12–ATG5-ATG16L1 complex in MDA-MB-231 cells with BIRC5 expression alterations (Figure 6B). Here, ectopic overexpression of BIRC5 decreased the amount of the cytoplasmic ATG12-ATG16L1 PLA puncta present in MDA-MB-231 and A549 cells, whereas, downregulation of BIRC5 by siRNA or by YM155 increased the amount of the cytoplasmic ATG12-ATG16L1 PLA puncta present in cells (Figure 6C,D and S10A). Similar to the results of the in situ PLA, immunoprecipitation of the endogenous ATG16L1 showed that ectopic overexpression of BIRC5 decreased the interactions between ATG16L1 and ATG12–ATG5 conjugate in MDA-MB-231 and A549 cells (Figure 6E and Figure S10B). Conversely, downregulation of

BIRC5 by siRNA increased the interactions between ATG16L1 and ATG12–ATG5 conjugate in cells (Figure 6E and Figure S10B). Taken together, these results support the in silico predicted effects of BIRC5 on the complexation between ATG12–ATG5 conjugate and ATG16L1.

Serum deprivation decreases BIRC5 expression and reduces the interactions between BIRC5, ATG12/ATG5-containing molecules in cancer cells

Given the abundance of free ATG12–ATG5 conjugate available, cells may still capable of forming ATG12–ATG5-ATG16L1 complex and upregulating autophagy without decreasing the expression of BIRC5 and/or forming extra ATG12–ATG5 conjugate by removing BIRC5 from the ATG12–ATG5-BIRC5 protein complex. Serum deprivation is known to promote autophagy in cells (Figure S11). Here, possible changes in BIRC5 expression and the interactions between BIRC5 and ATG12–ATG5 conjugate were determined in cells cultured under serum deprivation conditions. Serum deprivation (2% FBS for 72 h) decreased the expression of BIRC5 and the amount of the cytoplasmic ATG12-BIRC5 and ATG5-BIRC5 PLA puncta present in MDA-MB-231 and A549 cells (Figure 7A,B). Corresponding with the predicted molecular autophagic effects of BIRC5, serum deprivations also increased the expression of ATG7 and ATG12–ATG5 conjugate, the conversion of LC3B-II, and the amount of the cytoplasmic ATG12-ATG16L1 PLA puncta present in cells (Figure 7A,B). Immunoprecipitation of the endogenous ATG16L1 showed that serum deprivations increased the interactions between ATG16L1 and ATG12–ATG5 conjugate in MDA-MB-231 cells, further supporting that serum deprivations promote the formation of the ATG12–ATG5-ATG16L1 protein complex (Figure 7C). In contrast, serum deprivations did not alter the amount of the cytoplasmic BIRC5-CASP3 PLA puncta present in MDA-MB-231 cells (Figure 7D). Notably, the red fluorescent BIRC5-CASP3 PLA puncta was not observed in MCF7 cells, which are known to be CASP3 deficient, confirming the target-specificity of the antibodies used in this assay (Figure 7D). Collectively, these results suggest that BIRC5 may exhibit differential binding/dissociation preferences on apoptotic/autophagic molecules during different cellular events.

BIRC5 downregulation induces autophagy-dependent DNA damage in human cancer and mouse embryonic fibroblast cells

Finally, we sought to confirm the importance of the BIRC5-autophagy pathway in DNA integrity maintenance in cancer

---

Figure 5. BIRC5 interacts with ATG12–ATG5 conjugate in cancer cells. (A) Lysates of MDA-MB-231 cells were immunoprecipitated with anti-BIRC5, anti-ATG5, or anti-ATG12 antibodies. Protein-protein interactions between BIRC5, ATG12–ATG5 conjugate, ATG12, and ATG5 were determined by western blotting. (B) Expression of ATG5/ATG5-containing protein complexes and ATG12/ATG12-containing protein complexes was visualized by immunofluorescent microscopy. Nucleus were countered stained blue by DAPI. (C) Endogenous physical interactions between the examined molecules in MDA-MB-231 cells were detected by in situ PLA (indicated by red fluorescent puncta) and visualized by fluorescence microscopy. The Atg12–Atg5 conjugate deficient atg5−/− MEF cells were used as an antibody-specificity control for the ATG12–ATG5 and ATG12-ATG16L1 PLA assays. Nucleus were counter stained blue by DAPI. (D) Cytoplasmic and nucleic proteins were isolated and extracted from MDA-MB-231 cells. The present of ATG12–ATG5 conjugate, ATG12, and ATG5 in the extracted cytoplasmic and nucleic protein fractions was determined by western blotting. GAPDH/Gapdh and LMNA (lamin A/C) were used as the internal control of the cytoplasmic and nucleic protein fraction, respectively. (E) Endogenous physical interactions between BIRC5, ATG5, and ATG12 in MDA-MB-231 cells were detected by in situ PLA (indicated by red fluorescent puncta) and visualized by fluorescent microscopy. Nucleus were counter stained blue by DAPI. Scale bars: 25 μm (B), 10 μm (C and E).
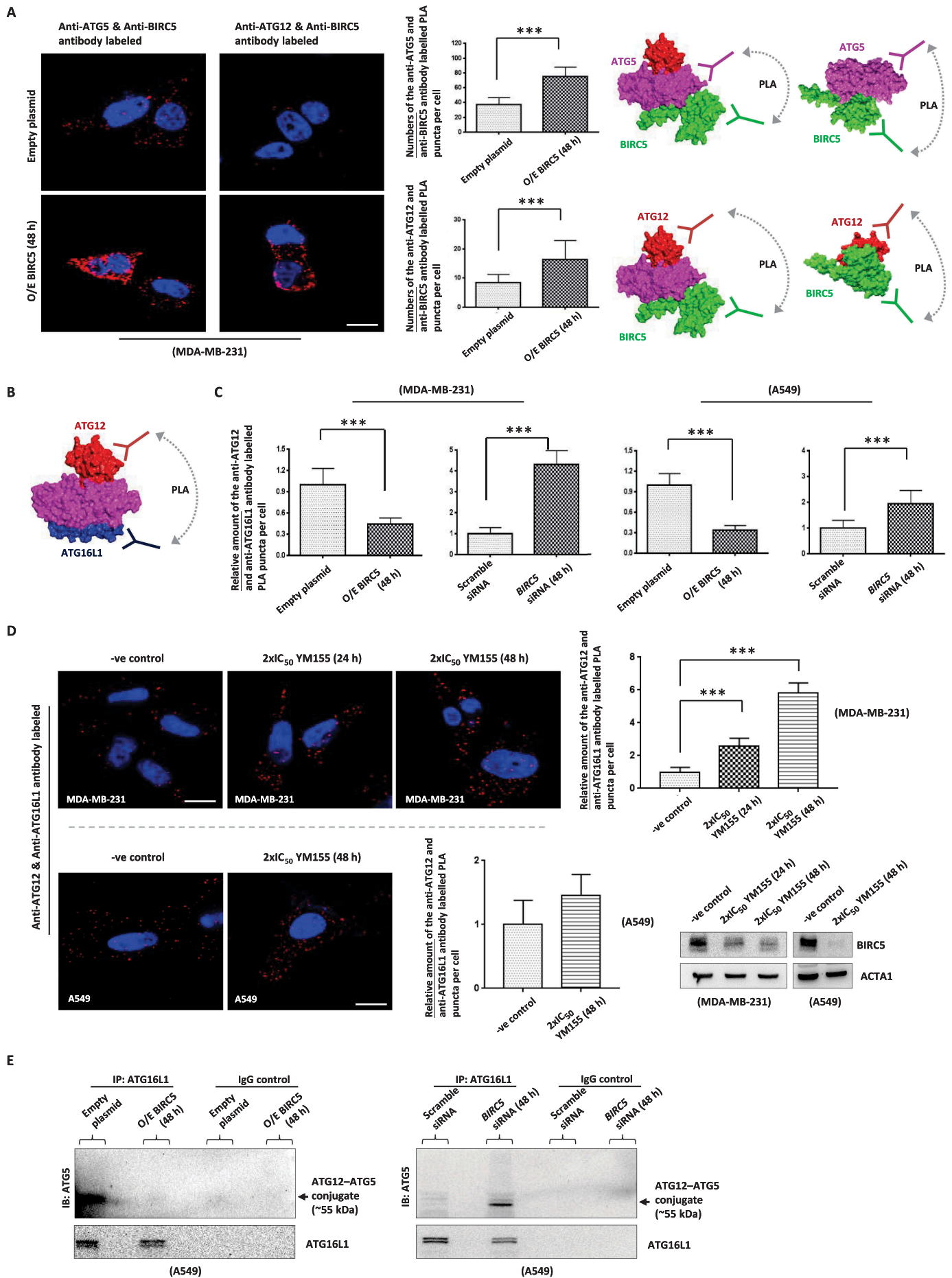
cells. We previously demonstrated that YM155 induced autophagy-dependent DNA damage in cancer cells [24]. Consistent with the previous findings, suppressing BIRC5 expression by YM155 induced DNA damage and co-incubation with the autophagy inhibitor, CQ (inhibits autophagosome maturation), partially attenuated the DNA damaging effects of YM155 in MCF7 and MDA-MB-231 cells under external stress-free conditions (Figure 8A). Here, co-incubation with autophagy inhibitors, CQ, 3-methyladenine (3MA, inhibits autophagosome formation), and bafilomycin A$_1$ (BAF, inhibits autophagosome maturation) also attenuated *BIRC5 (or Birc5)* siRNA-induced DNA damage in MCF7, MDA-MB-231, and MEF cells (Figure 8B,C). Moreover, results of the western blot analysis showed that co-incubation with CQ (and co-transfection with *LC3B* siRNA) attenuated *BIRC5* siRNA induced p-H2AX/γH2AX expression (a DNA damage marker) in MDA-MB-231 cells (Figure 8D, **top and middle panels**). Co-transfection with *Lc3b* siRNA also partially attenuated the effects of *Birc5* siRNA on p-H2AX expression in MEF cells (Figure 8D, **bottom panel**). Noticeably, downregulation of mouse *Birc5* by siRNA only increased the expression of p-H2AX in MEF cells but not in the autophagy-deficient *atg5*$^{-/-}$ MEF cells (Figure 8E). These results support the model that BIRC5 maintains DNA integrity in part through autophagy regulations in human cancer and mouse embryonic fibroblast cells.

Discussion

Apoptosis and autophagy were initially thought to be two mutually exclusive cellular events; however, emerging evidence suggests that crosstalk between mitosis, apoptosis, and autophagy plays an important role in supporting cancer cell survival and proliferation [39,40]. However, the detailed mechanistic connections between these important cellular events remain poorly understood.

During autophagy, multiple ATG proteins including ATG5, ATG7, ATG10, ATG12, and LC3 (mammalian Atg8 homologue) are recruited to the phagophore for autophagosome formation. ATG7 is a multi-role E1-like enzyme that facilitates LC3-lipidation, activates ATG12, and transfers the activated ATG12 to ATG10, which is an E2-like enzyme that facilitates the subsequent ATG12–ATG5 conjugation. One of the functions of ATG12–ATG5 conjugate is to promote LC3-lipidation [32]. The other function of ATG12–ATG5 conjugate is to provide a platform for the complex formation of ATG12–ATG5-ATG16L1 [34]. In fact, ATG12–ATG5 conjugation (and the following ATG12–ATG5-ATG16L1 complexation) and LC3-lipidation are both essential for autophagosome formation during canonical autophagy [38,41]. In this study, we found that BIRC5, which is a well-known

apoptosis inhibitor and mitosis positive-regulator, negatively modulates autophagy in part through expression and protein stability alterations of ATG7 and physical interactions with ATG12–ATG5 conjugate in cancer cells.

Despite the unconjugated-ATG12 and ATG5 monomer were not found in the BIRC5-containing immune complexes extracted from MDA-MB-231 and A549 cells, results of the *in situ* PLA suggest that the ATG12-BIRC5 and ATG5-BIRC5 protein complex existed possibly in the nucleus of cells. However, it is unclear on whether the physical interactions between BIRC5, ATG12, and ATG5 monomer in the nucleus play an important role in the regulation of autophagy, given that ATG12 and ATG5 mostly appear as ATG12–ATG5 conjugate (and ATG12–ATG5-ATG16L1 complex) in the cytoplasm. Moreover, Maskey *et al.* demonstrated that nuclear ATG5 interacts with BIRC5 and displaces BIRC5 from the CPC complex, leading to the induction of mitotic catastrophe in the DNA-damaging agents-treated Jurkat T cells [42]. Thus, nuclear ATG5 can modulate the mitotic functions of BIRC5 under certain circumstances. It is also important to point out that LC3 is present both in the cytoplasm and the nucleus, and deacetylation of nuclear LC3 induces its cytoplasmic translocation, where it can associate with ATG7 and other autophagic factors to promote autophagy [43]. Further investigations are required to determine whether nuclear BIRC5 can counter-regulate the formation of ATG12–ATG5 conjugate through physical interactions with nuclear ATG5/ATG12 and inhibition of their cytoplasmic translocation in cells.

BIRC5 may also interfere with the process of autophagy through ATG family proteins-unrelated mechanisms. Similar to BIRC5, XIAP/BIRC4 (X-linked inhibitor of apoptosis) is a member of the IAPs family. Even though this IAPs family member is known as a potent apoptosis inhibitor, a study by Huang *et al.* revealed that XIAP inhibits autophagy *via* an MDM2/Mdm2 (MDM2 proto-oncogene)-TP53 signaling pathway in wild type (WT) TP53-expressing cancer cells [44]. Consider that BIRC5 binds to DIABLO/SMAC (diablo IAP-binding mitochondrial protein, also known as SMAC) and negatively modulates the inhibitory effect of DIABLO on XIAP [45–47], BIRC5 may also indirectly regulate autophagy through a DIABLO-XIAP-MDM2-TP53 pathway in WT TP53-expressing cells.

From physiological perspectives, upregulation of BIRC5 and autophagy (*i.e.* to certain levels) can both promote cells survival in the presence of external stresses. Therefore, it is surprising to discover that BIRC5 negatively modulates ATG7 protein stability and autophagy in human cancer and MEF

Figure 6. BIRC5 modulates the formation of ATG12–ATG5-ATG16L complex in cancer cells. (A) MDA-MB-231 cells were transfected with either the empty plasmid DNA or the BIRC5 expressing plasmid DNA for 48 h. Physical interactions between BIRC5, ATG5, and ATG12 were detected by *in situ* PLA (indicated by red fluorescent puncta) and visualized by fluorescent microscopy. Nucleus were counter stained blue by DAPI. A statistically significant difference in the numbers of protein-protein interacting complex in cells transfected with the empty plasmid DNA *vs.* the BIRC5-expressing plasmid DNA is denoted by "***" ($p < 0.001$). (B) Schematic diagram showing the examined protein complex by *in situ* PLA. (C) MDA-MB-231 and A549 cells were transfected with the empty plasmid DNA, BIRC5-expressing plasmid DNA, scramble siRNA, or *BIRC5* siRNA for 48 h. Physical interactions between ATG12 and ATG16L1 were detected by *in situ* PLA. Representative photos are shown in Fig S10A. (D) Cells were treated with or without YM155 for 24 and 48 h. Physical interactions between ATG12 and ATG16L1 were detected by *in situ* PLA. A statistically significant difference in the numbers of ATG12-ATG16L1 interacting complex in cells between the testing groups is denoted by "***" ($p < 0.001$). (E) Cells were transfected with the empty plasmid DNA, BIRC5 expressing plasmid DNA, scramble siRNA, or *BIRC5* siRNA for 48 h. Lysates of A549 cells were immunoprecipitated with anti-ATG16L1 antibodies. Protein-protein interactions between ATG16L1 and ATG12–ATG5 conjugate were determined by western blotting. Scale bars: 15 μm (A and D).
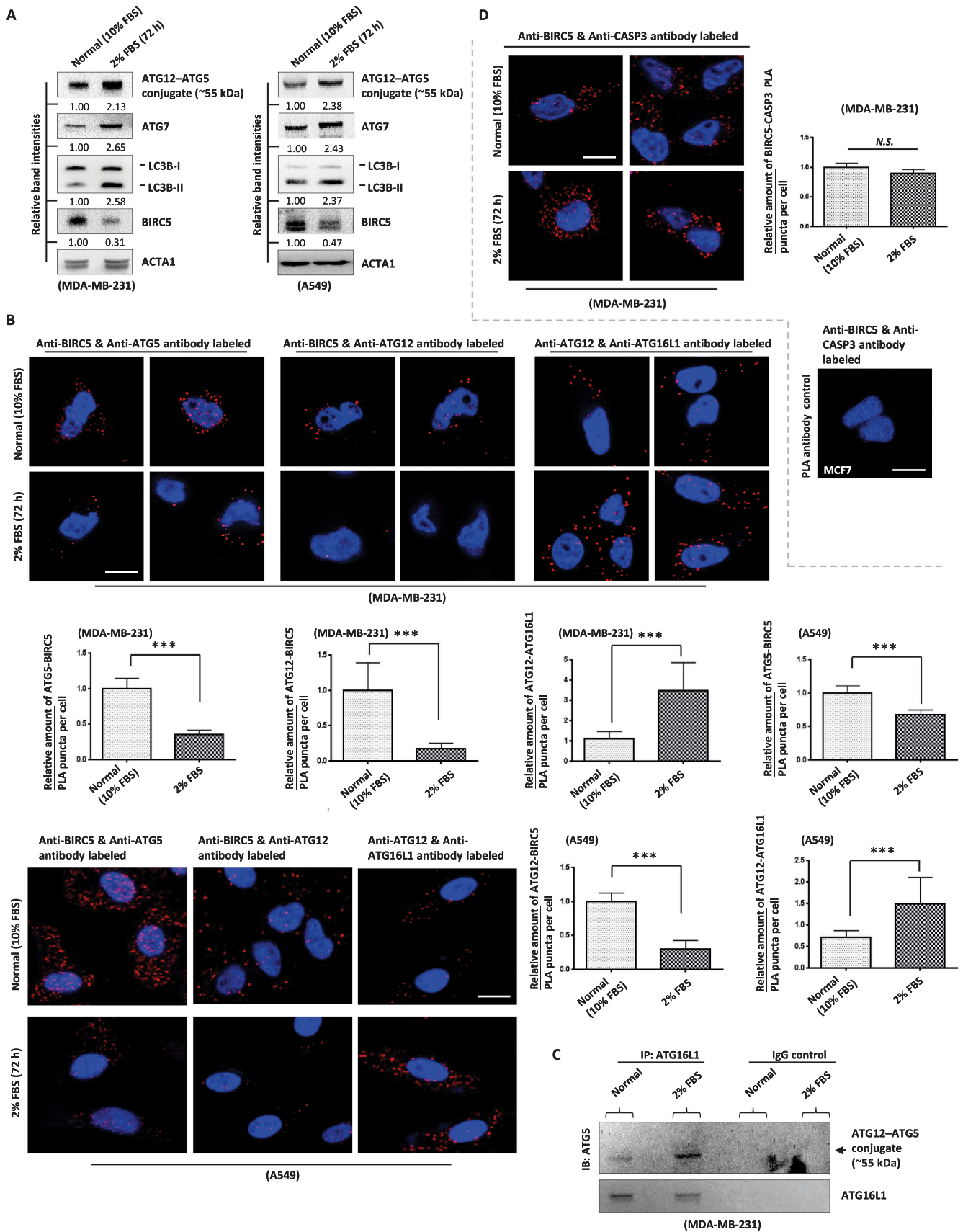
Figure 7. Serum deprivation decreases BIRC5 expression and BIRC5-ATG5/BIRC5-ATG12 interactions in cancer cells. (A) MDA-MB-231 and A549 cells were cultured under normal (10% FBS) and serum deprived (2% FBS) conditions for 72 h. Expression of different proteins was determined by western blotting. ACTA1 was used as an internal control. (B) MDA-MB-231 and A549 cells were cultured under either normal (10% FBS) or serum deprived (2% FBS) conditions for 72 h. Physical interactions between BIRC5, ATG5, ATG12, and ATG16L1 were determined by the *in situ* PLA. A "***" denotes a statistical differences (*P* < 0.0001) existed between the testing groups. (C) MDA-MB-231 cells were cultured under either normal (10% FBS) or serum deprived (2% FBS) conditions for 72 h. Lysates of cells were immunoprecipitated with anti-ATG16L1 antibodies. Protein-protein interactions between ATG16L and ATG12–ATG5 conjugate were determined by western blotting. (D) MDA-MB-231 cells were cultured under either normal (10% FBS) or serum deprived (2% FBS) conditions for 72 h. Physical interactions between BIRC5 and CASP3 were determined by the *in situ* PLA. The *CASP3*-deficient MCF7 cells were used as an antibody-specificity control for the BIRC5-CASP3 PLA assay. Nucleus were countered stained blue by DAPI. Scale bars: 15 μm (B and D).
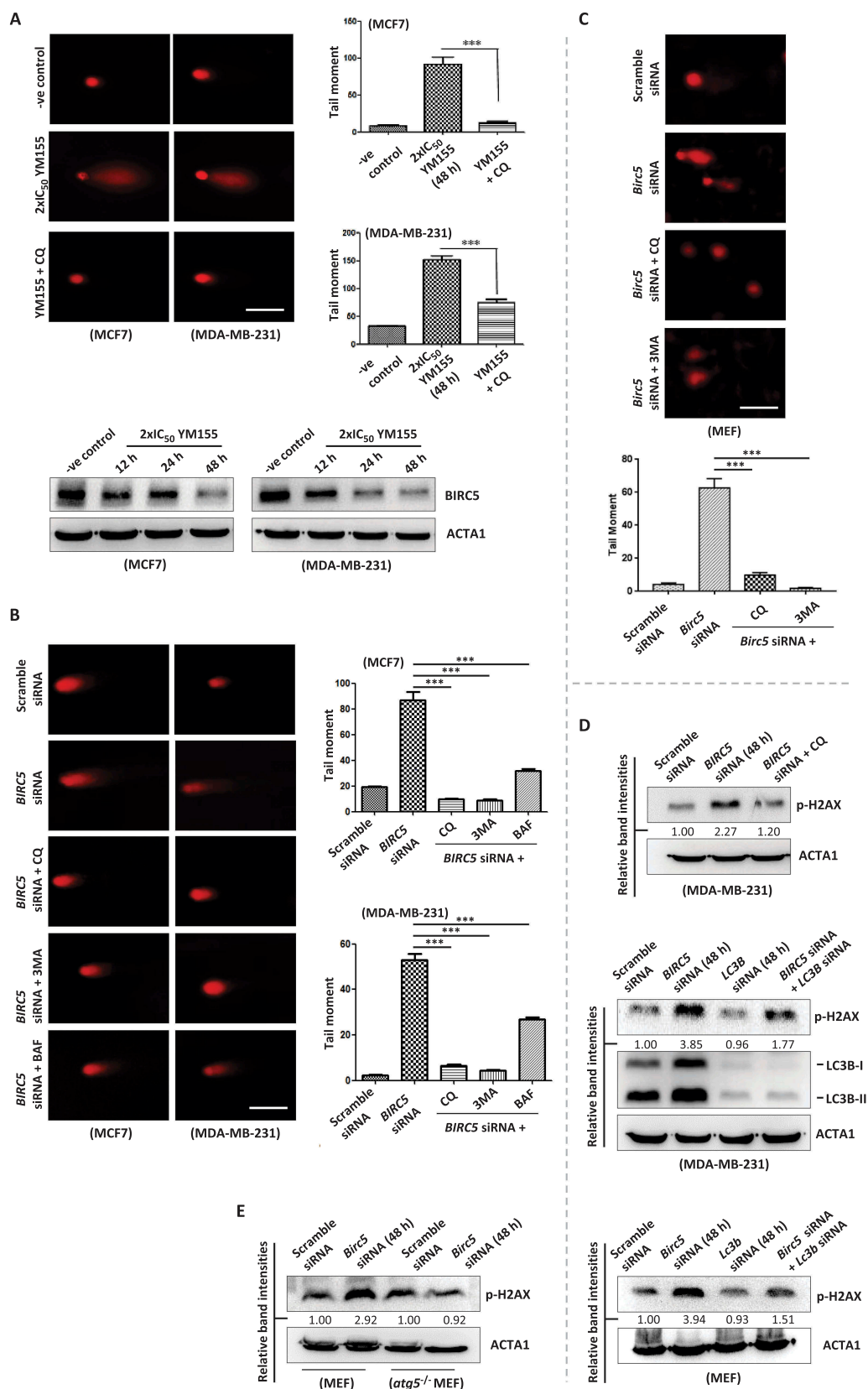
Figure 8. BIRC5 downregulation induces autophagy-dependent DNA damage in human cancer and mouse embryonic fibroblast cells. (A) MCF7 and MDA-MB-231 cells were treated with or without 2xIC$_{50}$ YM155 and co-incubated with or without CQ for 48 h. DNA damage was detected using comet assay. A statistically significant difference ($P < 0.0001$) in the relative tail moment of cells treated with YM155 versus YM155 + CQ is denoted by a "***". (B and C) MCF7, MDA-MB-231, and MEF cells were transfected with either scramble siRNA or *BIRC5* (*Birc5*) siRNA and co-incubated with or without CQ (15 µM), 3MA (4 mM), and BAF (3 nM) for 48 h. DNA damage was detected using comet assay. A statistically significant difference ($P < 0.0001$) in the relative tail moment of cells treated with *BIRC5* (*Birc5*) siRNA versus *BIRC5* (*Birc5*) siRNA + CQ/3MA/BAF is denoted by a "***". (D) MDA-MB-231 and MEF cells were transfected with either scramble siRNA or *BIRC5* (*Birc5*) siRNA and co-incubated with or without CQ (15 µM) or *LC3B* (*Lc3b*) siRNA transfection for 48 h. Expression of p-H2AX was examined by western blot analysis. (E) MEF and *atg5*$^{-/-}$ MEF cells were transfected with either scramble siRNA or *Birc5* siRNA for 48 h. Expression of p-H2AX was examined by western blot analysis. Scale bars: 50 µm (A, B, and C).

cells in this study. A possible reason for having BIRC5 to suppress and to maintain autophagy at certain levels in cells under "non-stressed conditions" is that hyperactivation of autophagy can cause excessive "self-digestion" and genomic instability, which may lead to cell death. Despite upregulation of autophagy has widely been shown to promote DNA repair in cells treated with different DNA damaging agents [48–50], other studies revealed that excessive autophagy could induce genomic instability in cancer cells. For example, excessive autophagy has been shown to decrease the activity of ribonucleotide reductase and the production of deoxyribonucleoside triphosphates (dNTPs), leading to the induction of genomic instability in human cancer cells [51,52]. Furthermore, Huang *et al.* demonstrated that targeting CTSS (cathepsin S) by small molecule inhibitors induced autophagy-dependent ROS production and the ROS-dependent DNA damage in HONE-1 cells [53]. Notably, we also demonstrated that targeting BIRC5 by YM155 (or siRNA) induced autophagy-dependent DNA damage in human cancer cells and MEF cells (Figure 8) and autophagic cell death in human breast cancer cells [24]. The autophagy negative-modulatory effects of BIRC5 may play an important role in maintaining the "cell cycle-required" amount of dNTPs and suppressing the excessive ROS production in cells. Given the roles of BIRC5 on multiple cellular processes, cancer cells may simultaneously, and differentially, regulate mitosis, apoptosis, and autophagy through differential regulations of the expression of BIRC5 and the protein-protein interactions between BIRC5 and its binding partners under different circumstances such as nutrient and dNTPs deprivations.

It is also worth noting that normal cells exhibit a relatively high baseline autophagic level as compared to cancer cells and downregulation of the baseline autophagic level (with unclear reasons) is believed to play an important role in promoting tumorigenesis, possibly through decreasing the DNA repair/damaged organelle recycling capacity in cells under various external stresses [54–56]. Interestingly, BIRC5 expression is mostly undetected in differentiated human cells under non-stressed conditions and upregulation of BIRC5 is known to promote tumorigenesis. Thus, besides inhibiting apoptosis, upregulation of BIRC5 may also promote the transformation of normal cells to tumor cells through lowering the baseline autophagic level of cells.

In conclusion, our findings provide new insights into the cellular and molecular functions of BIRC5 in cancer cells (Figure 9). Recently, BIRC5 is a "hot" molecular target for the development of cancer therapeutics. Our findings can aid the clinical development of a variety of BIRC5-directly/indirectly targeted anti-cancer therapies currently under pre-clinical and clinical investigations (*e.g.* LLP3 [BIRC5 protein-protein interactions disruptor] [57]; sPD1/MS [soluble PDCD1/PD-1 fused MUC1/Mucin 1- and BIRC5-targeting DNA vaccine] [58]; PTX-SUR NPs [paclitaxel and *BIRC5* siRNA co-loaded smart polymeric nanoparticles] [59]; Simvastatin [3-hydroxy-3-methylglutaryl-coenzyme A reductase inhibitor] [60]; DHS
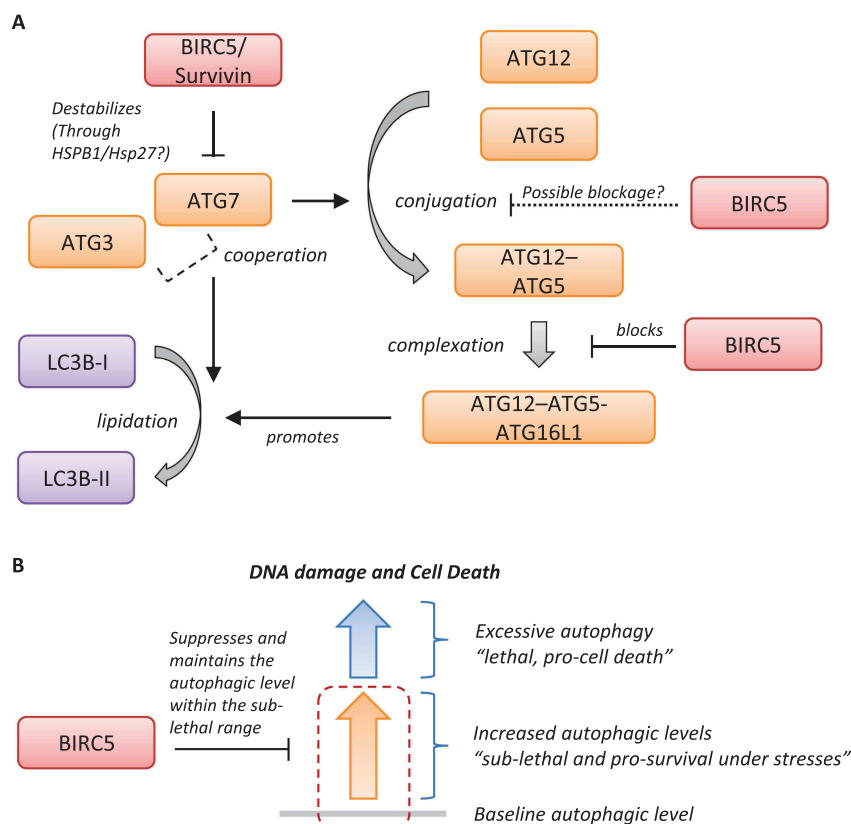
Figure 9. Schematic diagram showing the autophagy negative-modulating functions of BIRC5 in mammalian cells. (A) Molecular mechanisms of BIRC5 on autophagy regulation. (B) Cellular importance of BIRC5 on autophagy regulation.

[resveratrol analogue – trans-4,4′-dihydroxystilbene] [61]; CEP-1347 [kinase inhibitor] [62]; and ClinicalTrials.gov identifiers: NCT02851056; NCT02785250), by a better mechanistic understanding of how BIRC5 influences therapeutic response.

Materials and methods

Cell lines and cell culture conditions

Human MCF7, MDA-MB-231 (breast adenocarcinoma), and A549 (lung carcinoma) cells were originally obtained from ATCC (HTB-22, HTB-26, and CCL-185). MEF WT and the atg5 knockout (atg5$^{-/-}$) MEF cells were kindly donated by Prof. Chih-Peng Chang (National Cheng Kung University, Taiwan). Briefly, MCF7 cells were maintained in α-MEM (Minimum Essential medium; Gibco, 12000–022) containing 5% fetal bovine serum (FBS), penicillin-streptomycin-glutamine (PSG; Biological industries, 03-031-1B) and insulin transferrin selenium (Roche, 11074547001). The MDA-MB-231 cell line was maintained in RPMI (Roswell Park Memorial Institute 1640 medium; Thermo Fisher Scientific, 31800–022) containing 10% FBS and PSG. A549, WT MEF, and atg5$^{-/-}$ MEF cells were cultured in DMEM (Dulbecco's Modified Eagle medium; BioConcept, 1-26P02-L) containing 10% FBS and PSG. All cell lines were incubated at 37°C in a humidified incubator containing 5% CO_2 in air. All cell lines were tested negative for mycoplasma contamination. The use of the aforementioned human cell lines in this study was approved by the review board of Ministry of Science and Technology (Taiwan) and the biosafety committee of National Cheng Kung University (Taiwan).

Western blot analysis

Cells were lysed using CelLytic^{TM} cell lysis Reagent (Sigma-Aldrich, C2978) containing 1 mM PMSF and 1 mM NaF with cocktail protease inhibitors (Roche, 04693159001) and phosphatase inhibitors (G-Biosciences, 1786–450). Equal amounts of protein were subjected to SDS-PAGE on a 10% gel. The resolved proteins were transferred onto a PVDF membrane (Millipore, IPVH00010), which was then exposed to 5% nonfat dried milk (Fonterra)/bovine serum albumin (BSA; Sigma-Aldrich, A2153) in TBST buffer (2.44 g/L Tris base [Calbiochem, 9210], 8.76 g/L NaCl [Calbiochem, 567441], 0.05% Tween® 20 [Calbiochem, 9480-OP], pH 7.4) for 1 h at room temperature before incubation overnight at 4°C with primary antibodies: anti-BIRC5 (R&D Systems, AF886); anti-ATG7 (Millipore, AB10511); anti-ATG12 (Gene Tex, GTX124181); anti-ATG5 (Millipore, MAB2605); anti-ATG16L1 (Millipore, ABC25); anti-LC3B (Origene, TA301543); anti-SQSTM1 (Gene Tex, GTX100685); anti-p-MTOR (Ser2448) (Cell Signaling, 2971); anti-p-H3-3A (Abcam, ab32107); anti-ACTA1/actin (Millipore, MAB1501). Then, the PVDF membranes were washed 3 times with TBST buffer before incubation for 1 h at room temperature with HRP-conjugated secondary antibodies. Immune complexes were detected with chemiluminescence reagents. The luminescence protein signals were detected by Luminescence Readers (FUJI LAS-100, Tokyo, Japan). Experiments were repeated at least 3 times.

Immunohistochemistry – breast cancer tissue array

The human breast cancer normal tissue array (60 cases; CBB3) was purchased from Super Bio Chips (South Korea). The expression of BIRC5, SQSTM1, and ATG7 was evaluated in breast cancer tissues and matched normal breast tissues using a standard immunohistochemistry protocol. The slides were incubated with primary antibody anti-BIRC5 (R&D Systems, AF886); anti-SQSTM1 (Gene Tex, GTX100685); anti-ATG7 (Millipore, AB10511) overnight at 4°C. Then, the tissue arrays were washed and subsequently incubated with a universal secondary antibody for 1 h at room temperature. The expression levels of BIRC5, SQSTM1 and ATG7 were semi-quantitatively assessed based on staining density and intensity using the immunoreactive score (IRS) as described previously [63]. Briefly, IRS = staining intensity × percentage of positive cells (PP). Staining intensity was categorized as: 0 = negative; 1 = weak; 2 = moderate; 3 = strong; PP was graded as 0 = 0%; 1 = 0-25%; 2 = 25-50%; 3 = 50-75%; 4 = 75-100%. IRS of each specimen was successfully appraised by two independent pathologists based on the scoring criteria.

Gene silencing by siRNA

Target-validated siRNA oligos were transfected into cancer cells using Lipofectamine® RNAiMAX reagent (Invitrogen, 13778–150). Briefly, MDA-MB-231, MCF7, A549, MEF, and atg5$^{-/-}$ MEF cells were seeded onto 6 cm dishes and cultured overnight in antibiotic-free medium. Either the scramble siRNA (Dharmacon, D-001206-13-05) or the BIRC5-specific siRNA oligomers (Cell Signaling Technology, 6351) were diluted in Opti-MEM® I medium (Thermo Fisher Scientific, 11058021) without serum, and then mixed with Lipfectamine® RNAiMAX transfection reagent, which was also diluted in Opti-MEM® I medium, for 20 min at room temperature. Cells were overlaid with the transfection mixture, and incubated for various durations.

Ectopic overexpression of BIRC5 and ectopic expression of mGFP-EGFP-LC3

The pCMV6-XL4 and pCMV6-XL4-BIRC5 plasmid DNAs (NM_001168.2) were purchased from OriGene Technologies. The ptfLC3 plasmid DNA was a gift from Tamotsu Yoshimori (Addgene, 21074; deposited by Yoshimori lab) [64]. Lipofectamine® 3000 (Thermo Fisher Scientific, L3000015) was used to transfect the plasmids purified by the EndoFree® Plasmid Mega Kit (Qiagen, 12381) into the targeted cancer cells. Briefly, 0.2×10^6 of MDA-MB-231, MCF7, and A549 cells were seeded onto 6 cm dishes overnight. On the next day, appropriate Lipofectamine® 3000 reagent was diluted in Opti-MEM® I medium without serum. Purified plasmid DNA was also diluted in the Opti-MEM® I medium without serum, and subsequently an appropriate amount of P300 reagent was added to the diluted plasmid DNA. Diluted plasmid DNA together with P300 reagent was then mixed with the diluted Lipofectamine® 3000 reagent (1:1 ratio) and incubated for 5 min at room temperature. The transfection mixture was overlaid onto the cells for various durations.

Monodansylcadaverine (MDC) staining

MDC staining of AVOs including lysosome and autolysosome was performed for autophagy analysis. MDA-MB-231 breast cancer cells were seeded onto 6 cm dishes and allowed overnight to adhere. On the following day, the cells were transfected with either pCMV6-XL4 (Empty) or pCMV6-XL4-BIRC5 (O/E BIRC5) plasmid for 48 h in the presence or absence of resveratrol. AVOs were labeled with 0.5 mM MDC (Sigma-Aldrich, D4008) in the phenol red-free RPMI at 37°C for 30 min AVOs in all cells were observed under a fluorescence microscope (Olympus, IX-71). All experiments were repeated at least 3 times.

RNA extraction and qRT-PCR analysis

Total RNA was extracted using TRIzol® reagent (Invitrogen, 15596–026) and cDNA was synthesized from total RNA (2 μg) using the RevertAid H Minus First strand cDNA synthesis Kit (Thermo Scientific, K1632). Quantitative real-time PCR was used to determine the relative mRNA expression levels of ATG7 in treated cells using the StepOnePlus™ PCR system. The target fragment was amplified using specific primers (Forward primer 5′-GATCCGGGGATTTCTTTCACG-3′; Reverse primer 5′-CAGCAATGTAAGACCAGTCAAGT-3′) and the Fast SYBR® Green Master Mix (Applied Biosystems, 4385612) according to the following protocol: preheating at 95°C for 20 s, 45 cycles at 95°C for 1 s and 60°C for 30 s, and then a dissociation curve performed at 95°C for 15 s, 60°C for 60 s, and 95°C for 15 s. The target genes were quantified using the comparative threshold cycle (Ct) values $2^{-\Delta\Delta Ct}$ method (Δ Ct = $Ct_{Target\ gene}$ − Ct_{Actin}, $\Delta\Delta$ Ct = Δ $Ct_{Treatment}$ − $\Delta Ct_{Control}$). Experiments were repeated at least three times.

Protein stability assay

To measure the rate of degradation of ATG7, MDA-MB-231 and A549 cells were treated with 10 μg/mL cycloheximide (CHX; Sigma-Aldrich, C7698) after treating with ectopic overexpression of BIRC5 for 48 h to prevent further protein synthesis. Whole cell extracts were prepared from samples taken at 12 h time interval until 36 h and the expression of ATG7 was determined by western blotting. The rate of degradation was in relative terms to the starting time point (i.e. 0 h post-CHX).

The immunoprecipitation (IP) assay

Immunoprecipitation assays were performed using the Pierce® Crosslink Magnetic IP/Co-IP Kit (Thermo Fisher Scientific, 88805) according to the manufacturer's instructions. Briefly, cells were plated onto 15 cm dishes and cultured till 70-80% confluence. The cells were then harvested in 0.5 mL of IP lysis buffer 15 min on ice. Centrifuge the lysate at ~13,000 × g for 10 min to pellet the cell debris. Transfer supernatant to a new tube for protein concentration. The equal lysates were incubated with 5 μg of primary antibodies – normal rabbit IgG (Millipore, 12–370), anti-BIRC5 (Thermo scientific, PA1-16836), anti-ATG12 (Gene Tex, GTX124181), and anti-ATG5 (Millipore, MAB2605) and then crosslinked onto the magnetic beads with

rotation for 1 h at room temperature. After removing the unbound sample and washing the magnetic beads for three times, the IP products were eluted in elution buffer.

Immunofluorescent microscopy

MDA-MB-231 and A549 cells were seeded on glass coverslips for 48 h. Cells were then fixed with 4% paraformaldehyde at room temperature for 15 min, washed three times with ice cold phosphate-buffered saline (PBS; 8 g/L NaCl [Calbiochem, 567441], 0.2 g/L KCl [Calbiochem, 529551], 1.44 g/L Na_2HPO_4 [Calbiochem, 56547], 0.24 g/L KH_2PO_4 [Calbiochem, 529568], pH 7.4), permeabilized with PBST (PBS containing 1% Triton X-100 [Calbiochem, 9410]) for 30 min, and blocked in solution containing 5% BSA (Sigma-Aldrich, A2153) for 1 h at room temperature. The cells were incubated with primary antibody (anti-ATG5 [Millipore, MAB2605]; anti-ATG12 [Gene Tex, GTX629815]) at 4°C overnight and washed 3 times with TBST, followed by incubation with secondary antibody for 1 h at room temperature. Cells were washed three times with TBST and the slides were mounted with glycerol-gelatin. Nuclei were counterstained blue with DAPI (Invitrogen, P36935). The images were taken by scanning confocal microscope (MPE, Olympus).

In situ proximity ligation assay (PLA) assay

In situ PLA was performed to visualize protein-protein interactions in MDA-MB-231 and A549 cells. Briefly, cells were seeded onto 3-cm dishes overnight for adherence with ~80% confluence. Cells were then washed with PBS twice, and fixed with 4% paraformaldehyde for 15 min at room temperature. The fixed cells were permeabilized with PBS containing 1% Triton X-100 (Calbiochem, 9410-OP) for 30 min, subsequently blocked in Blocking Solution (Sigma-Aldrich, DUO82007) at 37°C for 1 h and incubated with primary antibodies (anti-BIRC5 [Cell Signaling Technology, 2808]; anti-ATG5 [Millipore, MAB2605; Gene Tex, GTX113309]; anti-ATG12 [Gene Tex, GTX629815], and anti-ATG16L1 [Millipore, ABC25]) overnight at 4°C. On the following day, cells were washed twice with washing buffer (Sigma-Aldrich, DUO82049), and incubated with PLA probes in a ratio of 1:5 in antibody diluent for 1 h at 37°C. The cells were then incubated with ligation solution at 37°C for 30 min and subsequently with amplification solution at 37°C for 100 min. Duolink in situ mounting medium (Sigma-Aldrich, DUO82040) together with DAPI were added to the cells at room temperature for 10 min. Cell images were captured with a confocal microscope (FV1000, Olympus).

Comet assays

Comet assays were carried out as previously described [24]. Microscopic slides were gently coated with 100 μL 1% normal melting point agarose (NMP; Vivantis Technologies, PC0701) using a coverslip and placed on ice for 15 min to allow the agarose to set. The coverslips were then removed. A 25-μL aliquot of the cell suspension (containing 10^5 cells) was gently mixed with 100 μL of 1.5% low melting point (37°C) agarose (UniRegion Bio-Tech, UR-AGA001) and pipetted onto the layer of 1% NMP agarose and re-covered with a coverslip. The coverslips were again removed and

the slides were lowered into freshly made ice cold lysis buffer (pH 10) containing 2.5 M NaCl, 100 mM EDTA, 10 mM Tris, and 1% Triton X-100 for 30 min. To allow DNA unwinding, the slides were placed into an electrophoresis chamber containing ice cold alkaline electrophoresis buffer containing 300 mM NaOH and 1 mM EDTA for 20 min. Electrophoresis was performed by setting the power supply to 25 V and adjusting the current to 300 mA for 20 min. After electrophoresis, the slides were placed in a freshly made neutralizing buffer (pH 7.5) containing 0.4 M Tris for 20 min. Cell staining was performed with 10 mL per slide of propidium iodide (20 mg/L; Sigma-Aldrich, P4170). The slides were examined with a fluorescence microscope (Optiphot-2, Nikon) at 20x magnification. Microscopy images of the comets were scored using TriTek CometScore™ Computer Software (Sumeduck). From each sample, one slide was prepared and the images of at least 100 cells from each slide were scored. The tail moment was chosen as our parameter for DNA damage. Experiments were repeated at least three times.

Computational modeling analysis – ZDOCK, RDOCK, and MD (molecular dynamics) simulation

Please refer to the supplementary information, S1.1–1.3, for details.

Statistical analysis

Each experiment was repeated at least three times. Data are presented as mean ± SEM. The significance of difference was evaluated with one-way analysis of variance (one-way ANOVA). A p-value < 0.05 was considered statistically significant.

Acknowledgments

Disclosure statement

Funding

ORCID

Tzu-Yu Lin http://orcid.org/0000-0003-1678-7779
Hsiu-Han Chan http://orcid.org/0000-0002-6843-4468
Shang-Hung Chen http://orcid.org/0000-0002-4086-4757
Sailu Sarvagalla http://orcid.org/0000-0001-7428-7663
Pai-Sheng Chen http://orcid.org/0000-0003-0513-1467
Mohane Selvaraj Coumar http://orcid.org/0000-0002-0505-568X
Siao Muk Cheng http://orcid.org/0000-0001-8145-4220
Yung-Chieh Chang http://orcid.org/0000-0002-8699-2834
Chun-Hui Lin http://orcid.org/0000-0002-7656-8095
Euphemia Leung http://orcid.org/0000-0002-6932-3188
Chun Hei Antonio Cheung http://orcid.org/0000-0003-4181-1435

References

[1] Levy JMM, Towers CG, Thorburn A. Targeting autophagy in cancer. Nat Rev Cancer. 2017;17:528.

[2] Ambrosini G, Adida C, Altieri DC. A novel anti-apoptosis gene, survivin, expressed in cancer and lymphoma. Nat Med. 1997;3(8):917–921.

[3] Zwerts F, Lupu F, De Vriese A, et al. Lack of endothelial cell survivin causes embryonic defects in angiogenesis, cardiogenesis, and neural tube closure. Blood. 2007;109(11):4742–4752.

[4] Jiang Y, de Bruin A, Caldas H, et al. Essential role for survivin in early brain development. J Neurosci. 2005;25(30):6962–6970.

[5] Wheatley SP, McNeish IA. Survivin: a protein with dual roles in mitosis and apoptosis. Int Rev Cytol. 2005;247:35–88.

[6] Coumar MS, Tsai F-Y, Kanwar JR, et al. Treat cancers by targeting survivin: just a dream or future reality? Cancer Treat Rev. 2013;39(7):802–811.

[7] Altieri DC. Survivin, cancer networks and pathway-directed drug discovery. Nat Rev Cancer. 2008;8(1):61–70.

[8] Fortugno P, Beltrami E, Plescia J, et al. Regulation of survivin function by Hsp90. Proc Natl Acad Sci U S A. 2003;100(24):13791–13796.

[9] Tran J, Master Z, Yu JL, et al. A role for survivin in chemoresistance of endothelial cells mediated by VEGF. Proc Natl Acad Sci U S A. 2002;99(7):4349–4354.

[10] Xie Y, Ma X, Gu L, et al. Prognostic and clinicopathological significance of survivin expression in renal cell carcinoma: a systematic review and meta-analysis. Sci Rep. 2016;6:29794.

[11] Huang W-T, Tsai Y-H, Chen S-H, et al. HDAC2 and HDAC5 up-regulations modulate survivin and miR-125a-5p expressions and promote hormone therapy resistance in estrogen receptor positive breast cancer cells. Front Pharmacol. 2017;8:902.

[12] Johnson EA, Svetlov SI, Pike BR, et al. Cell-specific upregulation of survivin after experimental traumatic brain injury in rats. J Neurotrauma. 2004;21(9):1183–1195.

[13] Cao W, Xie Y-H, Li X-Q, et al. Burn-induced apoptosis of cardiomyocytes is survivin dependent and regulated by PI3K/Akt, p38 MAPK and ERK pathways. Basic Res Cardiol. 2011;106(6):1207–1220.

[14] Levkau B, Schäfers M, Wohlschlaeger J, et al. Survivin determines cardiac function by controlling total cardiomyocyte number. Circulation. 2008;117(12):1583–1593.

[15] Yao -L-L, Wang Y-G, Cai W-J, et al. Survivin mediates the anti-apoptotic effect of delta-opioid receptor stimulation in cardiomyocytes. J Cell Sci. 2007;120(Pt 5):895–907.

[16] Shin S, Sung BJ, Cho YS, et al. An anti-apoptotic protein human survivin is a direct inhibitor of caspase-3 and-7. Biochemistry. 2001;40(4):1117–1123.

[17] Tamm I, Wang Y, Sausville E, et al. IAP-family protein survivin inhibits caspase activity and apoptosis induced by Fas (CD95), Bax, caspases, and anticancer drugs. Cancer Res. 1998;58(23):5315–5320.

[18] Vader G, Kauw JJW, Medema RH, et al. Survivin mediates targeting of the chromosomal passenger complex to the centromere and midbody. EMBO Rep. 2006;7(1):85–92.

[19] Rosa J, Canovas P, Islam A, et al. Survivin modulates microtubule dynamics and nucleation throughout the cell cycle. Mol Biol Cell. 2006;17(3):1483–1493.

[20] Sasai K, Katayama H, Hawke DH, et al. Aurora-C interactions with survivin and INCENP reveal shared and distinct features compared with aurora-B chromosome passenger protein complex. PLoS One. 2016;11(6):e0157305.

[21] Dai D, Liang Y, Xie Z, et al. Survivin deficiency induces apoptosis and cell cycle arrest in HepG2 hepatocellular carcinoma cells. Oncol Rep. 2012;27(3):621–627.

[22] Nakahara T, Takeuchi M, Kinoyama I, et al. YM155, a novel small-molecule survivin suppressant, induces regression of established human hormone-refractory prostate tumor xenografts. Cancer Res. 2007;67(17):8014–8021.

[23] Aoyama Y, Kaibara A, Takada A, et al. Population pharmacokinetic modeling of sepantronium bromide (YM155), a small molecule survivin suppressant, in patients with non-small cell lung cancer, hormone refractory prostate cancer, or unresectable stage III or IV melanoma. Invest New Drugs. 2013;31(2):443–451.

[24] Cheng SM, Chang YC, Liu CY, et al. YM155 down-regulates survivin and XIAP, modulates autophagy and induces autophagy-dependent DNA damage in breast cancer cells. Br J Pharmacol. 2015;172(1):214–234.

[25] Wang Y-F, Zhang W, He K-F, et al. Induction of autophagy-dependent cell death by the survivin suppressant YM155 in salivary adenoid cystic carcinoma. Apoptosis. 2014;19(4):748–758.

[26] Véquaud E, Séveno C, Loussouarn D, et al. YM155 potently triggers cell death in breast cancer cells through an autophagy-NF-kB network. Oncotarget. 2015;6:13476–13486.

[27] Eytan DF, Snow GE, Carlson S, et al. SMAC mimetic birinapant plus radiation eradicates human head and neck cancers with genomic amplifications of cell death genes FADD and BIRC2. Cancer Res. 2016;76(18):5442–5454.

[28] Lin K-Y, Cheng SM, Tsai S-L, et al. Delivery of a survivin promoter-driven antisense survivin-expressing plasmid DNA as a cancer therapeutic: a proof-of-concept study. Onco Targets Ther. 2016;9:2601–2613.

[29] Klionsky DJ, Abdelmohsen K, Abe A, et al. Guidelines for the use and interpretation of assays for monitoring autophagy (3rd edition). Autophagy. 2016;12(1):1–222.

[30] Ichimura Y, Kirisako T, Takao T, et al. A ubiquitin-like system mediates protein lipidation. Nature. 2000;408(6811):488–492.

[31] Park D, Norris KJ, Gibson G, et al. Resveratrol induces autophagy by directly inhibiting mTOR through ATP competition. Sci Rep. 2016;6:21772.

[32] Hanada T, Noda NN, Satomi Y, et al. The Atg12-Atg5 conjugate has a novel E3-like activity for protein lipidation in autophagy. J Biol Chem. 2007;282(52):37298–37302.

[33] Otomo C, Metlagel Z, Takaesu G, et al. Structure of the human ATG12~ATG5 conjugate required for LC3 lipidation in autophagy. Nat Struct Mol Biol. 2012;20:59.

[34] Romanov J, Walczak M, Ibiricu I, et al. Mechanism and functions of membrane binding by the Atg5-Atg12/Atg16 complex during autophagosome formation. Embo J. 2012;31(22):4304–4317.

[35] Chen S-F, Chang -C-C, Wu C-H, et al. Autophagy-related gene 7 is downstream of heat shock protein 27 in the regulation of eye morphology, polyglutamine toxicity, and lifespan in Drosophila. J Biomed Sci. 2012;19(1):52.

[36] Li J, Tang C, Li L, et al. Quercetin blocks t-AUCB-induced autophagy by Hsp27 and Atg7 inhibition in glioblastoma cells in vitro. J Neurooncol. 2016;129(1):39–45.

[37] Matsushita M, Suzuki NN, Fujioka Y, et al. Expression, purification and crystallization of the Atg5-Atg16 complex essential for autophagy. Acta Crystallogr Sect F Struct Biol Cryst Commun. 2006;62(Pt 10):1021–1023.

[38] Matsushita M, Suzuki NN, Obara K, et al. Structure of Atg5·Atg16, a complex essential for autophagy. J Biol Chem. 2007;282(9):6763–6772.

[39] Pattingre S, Tassa A, Qu X, et al. Bcl-2 antiapoptotic proteins inhibit beclin 1-dependent autophagy. Cell. 2005;122(6):927–939.

[40] Scherz-Shouval R, Weidberg H, Gonen C, et al. p53-dependent regulation of autophagy protein LC3 supports cancer cell survival under prolonged starvation. Proc Natl Acad Sci U S A. 2010;107(43):18511–18516.

[41] Walczak M, Martens S. Dissecting the role of the Atg12-Atg5-Atg16 complex during autophagosome formation. Autophagy. 2013;9(3):424–425.

[42] Maskey D, Yousefi S, Schmid I, et al. ATG5 is induced by DNA-damaging agents and promotes mitotic catastrophe independent of autophagy. Nat Commun. 2013;4:2130.

[43] Huang R, Xu Y, Wan W, et al. Deacetylation of nuclear LC3 drives autophagy initiation under starvation. Mol Cell. 2015;57(3):456–466.

[44] Huang X, Wu Z, Mei Y, et al. XIAP inhibits autophagy via XIAP-Mdm2-p53 signalling. Embo J. 2013;32(16):2204–2216.

[45] Sun C, Nettesheim D, Liu Z, et al. Solution structure of human survivin and its binding interface with Smac/Diablo. Biochemistry. 2005;44(1):11–17.

[46] Liu Z, Sun C, Olejniczak ET, et al. Structural basis for binding of Smac/DIABLO to the XIAP BIR3 domain. Nature. 2000;408(6815):1004–1008.

[47] Srinivasula SM, Hegde R, Saleh A, et al. A conserved XIAP-interaction motif in caspase-9 and Smac/DIABLO regulates caspase activity and apoptosis. Nature. 2001;410(6824):112–116.

[48] Ge R, Liu L, Dai W, et al. 652 XPA promotes autophagy to facilitate cisplatin resistance in melanoma cells through the activation of PARP1. J Invest Dermatol. 2016;136(5):S115–S115.

[49] Xu F, Li X, Yan L, et al. Autophagy promotes the repair of radiation-induced DNA damage in bone marrow hematopoietic cells via enhanced STAT3 signaling. Radiat Res. 2017;187(3):382–396.

[50] Wang YN, Zhang N, Zhang L, et al. Autophagy regulates chromatin ubiquitination in DNA damage response through elimination of SQSTM1/p62. Mol Cell. 2016;63(1):34–48.

[51] Chen W, Zhang L, Zhang K, et al. Reciprocal regulation of autophagy and dNTP pools in human cancer cells. Autophagy. 2014;10(7):1272–1284.

[52] Chen Y-R, Tsou B, Hu S, et al. Autophagy induction causes a synthetic lethal sensitization to ribonucleotide reductase inhibition in breast cancer cells. Oncotarget. 2016;7(2):1984–1999.

[53] Huang -C-C, Chen K-L, Cheung CHA, et al. Autophagy induced by cathepsin S inhibition induces early ROS production, oxidative DNA damage, and cell death via xanthine oxidase. Free Radic Biol Med. 2013;65:1473–1486.

[54] Kongara S, Kravchuk O, Teplova I, et al. Autophagy regulates keratin 8 homeostasis in mammary epithelial cells and in breast tumors. Mol Cancer Res. 2010;8(6):873.

[55] Liu H, He Z, von Rutte T, et al. Down-regulation of autophagy-related protein 5 (ATG5) contributes to the pathogenesis of early-stage cutaneous melanoma. Sci Transl Med. 2013;5(202):202ra123.

[56] Cho D-H, Jo YK, Kim SC, et al. Down-regulated expression of ATG5 in colorectal cancer. Anticancer Res. 2012;32(9):4091–4096.

[57] Steigerwald C, Rasenberger B, Christmann M, et al. Sensitization of colorectal cancer cells to irinotecan by the survivin inhibitor LLP3 depends on XAF1 proficiency in the context of mutated p53. Arch Toxicol. 2018;92(8):2645–2648.

[58] Liu CL, Lu Z, Xie Y, et al. Soluble PD-1-based vaccine targeting MUC1 VNTR and survivin improves anti-tumor effect. Immunol Lett. 2018;200:33–42.

[59] Jin MJ, Jin G, Kang L, et al. Smart polymeric nanoparticles with pH-responsive and PEG-detachable properties for co-delivering paclitaxel and survivin siRNA to enhance antitumor outcomes. Int J Nanomedicine. 2018;13:2405–2426.

[60] Cai W-Y, Zhuang Y, Yan F, et al. Effect of survivin downregulation by simvastatin on the growth and invasion of salivary adenoid cystic carcinoma. Mol Med Rep. 2018;18(2):1939–1946.

[61] Saha B, Pai GB, Subramanian M, et al. Resveratrol analogue, trans-4,4′-dihydroxystilbene (DHS), inhibits melanoma tumor growth and suppresses its metastatic colonization in lungs. Biomed Pharmacother. 2018;107:1104–1114.

[62] TOGASHI K, Okada M, Yamamoto M, et al. A small-molecule kinase inhibitor, CEP-1347, inhibits survivin expression and sensitizes ovarian cancer stem cells to paclitaxel. Anticancer Res. 2018;38(8):4535–4542.

[63] Fedchenko N, Reifenrath J. Different approaches for interpretation and reporting of immunohistochemistry analysis results in the bone tissue - a review. Diagn Pathol. 2014;9:221.

[64] Kimura S, Noda T, Yoshimori T. Dissection of the autophagosome maturation process by a novel reporter protein, tandem fluorescent-tagged LC3. Autophagy. 2007;3(5):452–460.